THE JOURNAL OF PHYSICAL CHEMISTRY C

Article

pubs.acs.org/JPCC

Structural and Morphological Study of a Poly(3-hexylthiophene)/Streptavidin Multilayer Structure Serving as Active Layer in Ultra-Sensitive OFET Biosensors

Maria Magliulo,[†,⊥,∥] Davide Altamura,[‡,∥] Cinzia Di Franco,[#,∥] Maria Vittoria Santacroce,[#] Kyriaki Manoli,[†,⊥] Antonia Mallardi,[§] Gerardo Palazzo,[†,⊥] Gaetano Scamarcio,[#] Cinzia Giannini,*[,‡] and Luisa Torsi*[,†,⊥]

[†]Dipartimento di Chimica, Università degli Studi di Bari "A. Moro", Via Orabona, 4, 70126 Bari Italy

[⊥]CSGI, Università degli Studi di Firenze, via della Lastruccia, 3, 50019 Sesto Fiorentino, Italy

[‡]Istituto di Crystallografia, CNR-IC, 70126 Bari Italy

[§]Istituto per i Processi Chimico-Fisici, CNR-IPCF, Via Orabona, 4, 70126 Bari Italy

[#]CNR-IFN and Dipartimento Interateneo di Fisica, Università degli Studi di Bari "A. Moro", Via Orabona, 4, 70126 Bari Italy

Supporting Information

ABSTRACT: Organic field-effect transistors including a functional biorecognition interlayer, sandwiched between the dielectric and the organic semiconductor layers, have been recently proposed as ultrasensitive label-free biosensors capable to detect a target molecule in the low pM concentration range. The morphology and the structure of the stacked bilayer formed by the protein biointerlayer and the overlying organic semiconductor is here investigated for different protein deposition methods. X-ray scattering techniques and scanning electron microscopy allow us to gather key relevant information on the interface structure and to assess target analyte molecules capability to percolate through the semiconducting layer reaching the protein deposit lying underneath. Correlations between the structural and morphological data and the device analytical performances are established allowing us to gather relevant details on the sensing mechanism and further improving sensor performances, in particular in terms of sensitivity and selectivity.

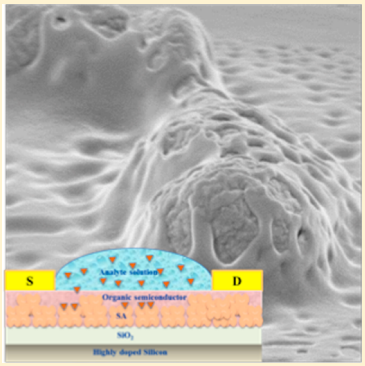

INTRODUCTION

Lately, biosensors based on organic field effect transistors have attracted a great deal of attention[1] as demonstrated also by the large number of papers published in this field. OFET sensors, proven to reach high performances especially as to sensitivity is concerned, can be useful in key relevant applications such as clinical diagnostic, drug analysis, environmental monitoring and food control.[2,3] More importantly, OFET biosensors can be fabricated on flexible plastic or even paper substrates, in principle at low-cost through processes compatible with printing techniques. This, together with the high performance level demonstrated, might open up perspectives in the production of high-throughput and disposable electronic sensors to be used in point-of-care or point-of-need medical applications.[4,5]

A typical OFET biosensor is composed of a core stacked layers structure composed of a dielectric, an organic semiconductor along with a system of biological recognition elements that are integrated into the device structure. Although a number of bioelectronic architectures have been considered to be used as biosensors, the most widely proposed structure envisages a biorecognition layer deposited on top of the organic semiconductor layer.[6−8] This approach, however, may result in not fully optimized performances as the biorecognition event can occur far from the region where the electronic transport takes place. With the aim of improving the device performance level, novel OFET biosensors, comprising a functional biological interlayer (FBI-OFET), were recently proposed.[9] In such structures (see Figure 1A) the biological recognition element layer lies underneath the organic semiconductor film, right at the interface where the OFET two-dimensional transport occurs.[9] Indeed, FBI-OFETs resulted in sensing devices with unprecedented performance level both in terms of sensitivity, reaching pM level, high selectivity, accuracy, and reproducibility. However, when the device is exposed to the molecules to be detected (target molecules), these need to percolate through the organic semiconductor layer to reach the protein layer, eventually giving rise to the recognition event that will be detected. This is recognized as one of the potential pitfall of an FBI-OFET structure as only very small target molecules are expected to easily and fast reach the recognition layer. In fact, this has been demonstrated not to be the case as

Received: May 12, 2014
Revised: June 26, 2014
Published: June 27, 2014

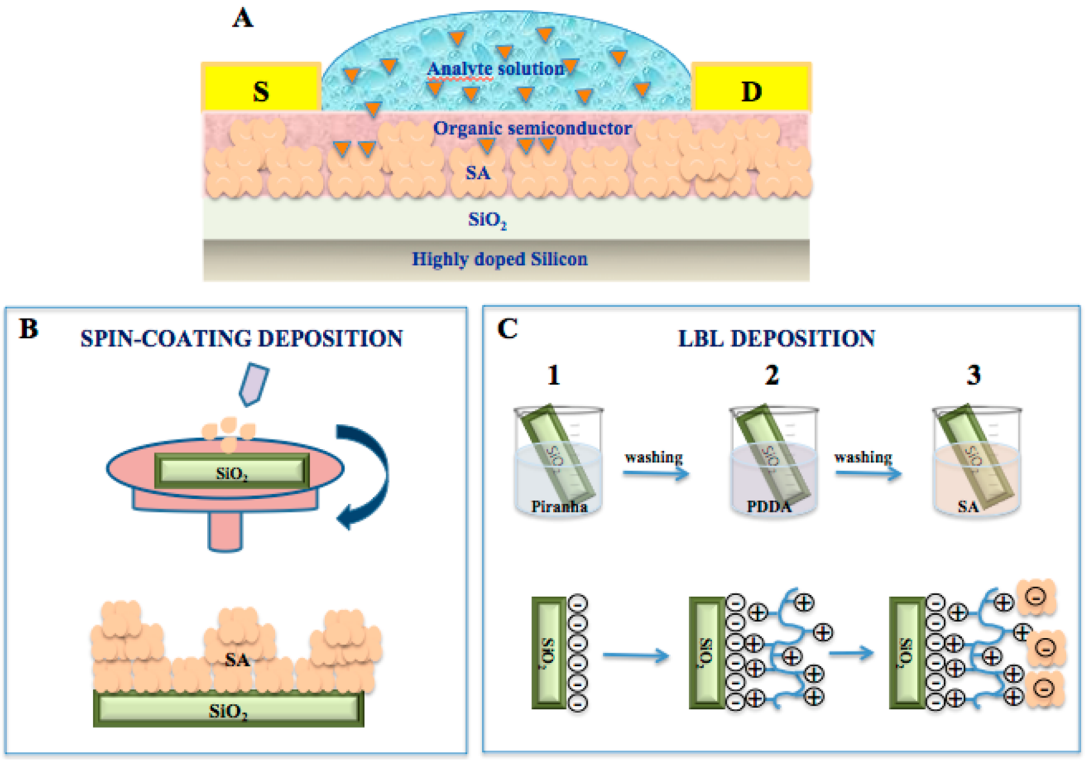

Figure 1. Schematic view of the FBI-OFET biosensor comprising a functional streptavidin interlayer directly deposited on the SiO_2 dielectric surface (A) by spin-coating (B) and layer by layer (C) deposition procedures. In the spin-coating procedure the protein solution is directly spread on the bare SiO_2 substrate after a piranha treatment aimed to increase the surface hydrophilicity (B). In the LbL deposition the SiO_2 substrate is first dipped in a piranha solution to obtain negative charges on the surface (step 1 in panel C), after washing, the substrate is dipped in the positively charged PDDA adhesion polymer solution (step 2 in panel C), finally the substrate is immersed in the negatively charged protein solution and the SA is electrostatically attached (step 3 in panel C). This procedure can be repeated several times to obtain the desired number of SA layers.

biomolecules such as insulin and even a large protein such as streptavidin, can flow through a 20 nm thick poly(3-hexylthiophene) - P3HT layer.[9] However, as things stand now, the reason for this occurrence is still not clear.

One of the FBI-OFET structures so far proposed, involves a P3HT based FBI-OFETs embedding a streptavidin (SA) capturing layer. They have been proposed as label-free, selective electronic sensors for biotin, exploiting the well know very strong SA-biotin binding constant.[10] The electrical and analytical performances of these OFET biosensors, assessed in previously published papers,[11,12] are extremely high. As anticipated, the biosensor is proven to reach extraordinary high sensitivities with detection limits of few part-per-trillion (or few tens of pM),[12] exhibiting also stable and repeatable responses. In these devices, the streptavidin capturing molecules are deposited on a silicon oxide dielectric surface through a spin-coating deposition process (Figure 1B) or an electrostatic layer-by-layer (LbL) assembly (Figure 1C).[13] It is well-known that the structure of a protein recognition layer anchored on silicon dioxide can affect the biosensors performance especially in terms of sensitivity and selectivity.[14] On the other hand, the morphology of the organic semiconductor is of great importance to fabricate OFET devices with high electronic performances particularly as to the field-effect mobility and I_{on}/I_{off} ratio is concerned.[15,16] In this respect, it is important to assess the FBI-OFET fabrication conditions that can lead to a stable SA-P3HT stacked structure. More importantly, it is critical that the properties and the quality of the dielectric/organic-semiconductor interface are controlled as they also strongly affect the device performance and stability.[17] Despite this, no study on the FBI-OFET interfacial morphological and structural properties has been proposed so far.

In this paper, the structural and the morphological features of the streptavidin/P3HT (SA/P3HT) stacked bilayer are investigated down to the nanoscale. Scanning electron microscopy (SEM), X-ray specular reflectivity (XSR), as well as grazing incidence small-angle X-ray scattering (GISAXS) allow us to study the organization and the degree of segregation of the SA biomolecules deposited by spin-coating and LbL assembly, before and after the P3HT organic semiconductor deposition. Important features on the P3HT morphology are also found that can explain why large biomolecules percolate through it. Moreover, the structure of the P3HT film is shown non to be affected by the different morphological features of the SA layer laying underneath, in agreement with the field-effect mobility not changing significantly when passing from a P3HT to a SA-P3HT OFET. In addition, the results of this analysis show that the spin-coating SA layer is characterized by an irregular morphology and a full substrate coverage whereas LbL leads to a nanostructured surface resembling a 2D network.

■ EXPERIMENTAL SECTION

A schematic of a FBI-OFET biosensor cross-sectional structure comprising a functional SA interlayer and a P3HT cover layer is reported in Figure 1A. The biotin analyte is delivered to the transistor electronic channel area by adding a 2 μL droplet of the biotin solution in water (HPLC grade).

Materials. Streptavidin (SA) and poly-(dimethyldiallylammonium chloride) (PDDA) were purchased from Sigma-Aldrich. Poly(3-hexylthiophene-2,5-diyl) (P3HT;

dx.doi.org/10.1021/jp504652u | J. Phys. Chem. C 2014, 118, 15853−15862

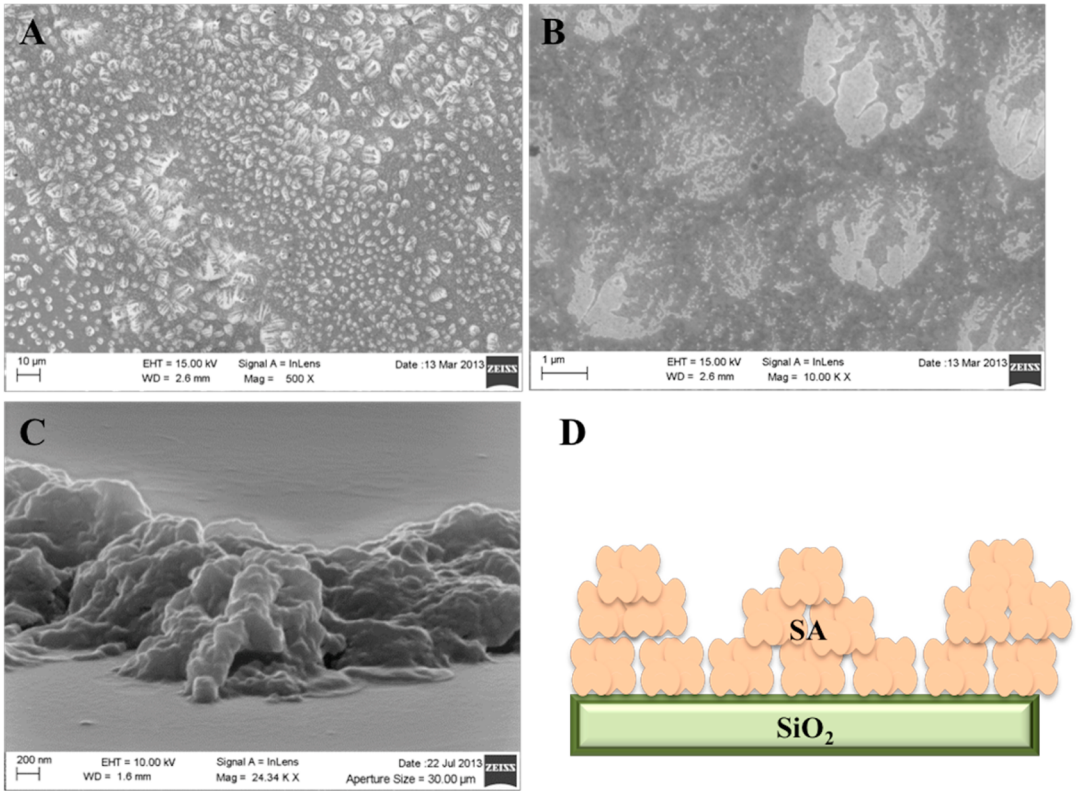

Figure 2. SEM images of the streptavidin layer obtained by spin-coating a 10 μg/mL protein solution on the SiO_2 dielectric surface. The images were acquired by using the In-lens detector at different magnification (A, B) and by tilting the sample of 75° (C). (D) Schematic of the presumed SA adsorption mechanism in the spin-coating deposition.

regioregularity >96% from Rieke Metals, Inc.) was purified as reported elsewhere.[18]

Protein Interlayer and Semiconductor Deposition. The streptavidin layers have been deposited, directly on the SiO_2 surface either by spin-coating or by layer-by-layer (LbL) deposition techniques, by using the same protocol as for the OFET biosensors fabrication.[12] Briefly, for the spin-coating procedure, 50 μL of a 10 μg/mL aqueous solution of SA, were spin deposited at 200 rpm for 40 min (Figure 1B). The concentration of the SA solution was optimized by fluorescent techniques to obtain a good surface coverage and an adequate number of binding sites. As reported previously,[12] the resulting SA film was 35 ± 5 nm thick and the estimated SA surface density was 10 pmol/cm^2, this being comparable to a fully packed SA monolayer (6.2 pmol/cm^2).[19]

As illustrated in Figure 1C, for the LbL deposition the SiO_2 surface was exposed to a "piranha" solution (oleum H_2SO_4 and H_2O_2, 7:3 v/v) for 15 min at 0 °C and was rinsed in water for 5 min, afterward. This procedure allows obtaining a hydrophilic, negatively charged SiO_2 surface (step 1 in Figure 1C). A first polycation layer was subsequently, electrostatically deposited on the negatively charged SiO_2 surface by placing the SiO_2 substrate in a 2 mg/mL poly(diallyl-dimethylammonium chloride) (PDDA)−water solution for 30 min (step 2 in Figure 1C). The sample was washed in water for 2 min and a layer of SA was adsorbed by dipping in a 100 μg/mL protein solution for 30 min (step 3 in Figure 1C). The PDDA/SA sample was rinsed with water and the two previously described steps were repeated a second time resulting in the PDDA/SA/PDDA/SA structure. The deposition of two SA layers allows obtaining the same amount of streptavidin molecules per unit area, ca. 10 pmol/cm^2, as for the spin-coating deposition process.[12] A better comparison between the two different SA deposition procedures is thus possible.

The P3HT organic semiconductor was deposited, directly on the SA layers or on SiO_2 surface, by spin-coating at 2000 rpm for 30 s. No SiO_2 surface silanization treatment to graft hydrophobic alkyl chain[20] was carried out before the P3HT deposition.

AFM and structural investigations performed on the P3HT deposited directly on the atomically flat SiO_2 shows that the morphology is composed of granular domains ca. 10−20 nm wide, along with voids of comparable size.[12]

Scanning Electron Microscopy (SEM) Characterization. The morphological characterization was performed by a ∑igma Zeiss field emission scanning electron microscope (FE-SEM). To avoid charging, the films were coated with an electron beam deposited thin palladium layer (10 ± 1 nm). The probing e-beam was set at an acceleration voltage of 5−15 kV and 10 and 30 μm slit apertures were used. SEM images were acquired by tilting the samples in a 0°−75° angle range and using the in-Lens detector.

X-ray Specular Reflectivity (XSR). XSR curves were collected by using a Bruker D8 Discover diffractometer, equipped with a Göbel mirror for the CuKα line, a scintillation detector, and an Eulerian cradle. XSR[21] probes the average electron density in a direction perpendicular to the substrate surface at the nanometric scale and allows investigating the structure of a buried layer or of an interface.[22] Reflectivity fringes signal can be seen only when the structures investigated comprise uniform features, such as segregated stacked layers or size monodispersed clusters forming a low roughness surface.

dx.doi.org/10.1021/jp504652u | J. Phys. Chem. C 2014, 118, 15853−15862

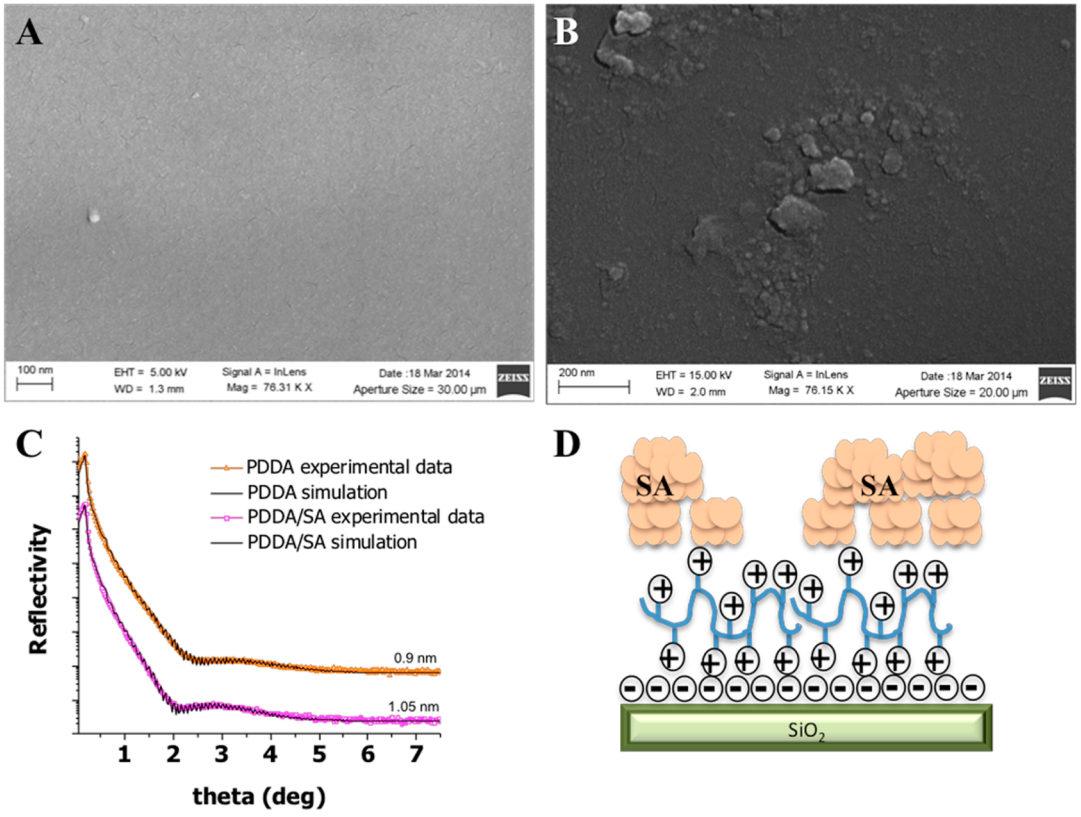

Figure 3. (A) SEM image for a PDDA adhesion polymer film deposited on a Si/SiO_2 substrate, the image was acquired after deposition of a 10 nm palladium layer; (B) SEM picture obtained for SA layers deposited by LbL assembly procedure on a Si/SiO_2 substrate, two layers of SA have been deposited; (C) XSR experimental (symbols) and simulated curves (black lines) for the PDDA adhesion polymer layer (orange curve) and LbL deposited SA (magenta curve). The actual thickness values as derived from the fit are reported next to each curve. (D) Schematic of the presumed SA adsorption mechanism in the LbL deposition.

GISAXS and GIWAXS. Grazing incidence small and wide angle scattering (GISAXS and GIWAXS) experiments were performed on a SMAX3000 system, coupled to a Rigaku FRE+ superbright rotating anode microsource (Cu Kα radiation).[23] GISAXS and GIWAXS data were collected on a Triton multiwire detector with 195 μm pixel size, and an image plate detector with 100 μm pixel size, respectively. To enhance the GISAXS signal a thin (10 ± 1 nm) palladium metal coating was deposited by electron beam evaporation on the samples. The GISAXS/GIWAXS data represent the X-ray diffracted intensity as a function of the scattering vector components, Qz and Qy, perpendicular and parallel to the sample surface, respectively.

RESULTS AND DISCUSSION

Morphology of the SA Protein Layers. SA has been selected as a model system for the development of FBI-OFET biosensors since this macromolecule is well characterized and the complex it forms with biotin is one of the strongest and most stable noncovalent interactions known.[24] The interaction between the SA protein and the SiO_2 surface must be strong enough to guarantee the formation of stable and possibly uniform coatings, which is seldom achieved when physisorption techniques are used. This holds true particularly when the physisorption is carried out by simple dipping of a SiO_2 surface into the protein solution[25,26] while better adhesion is usually achieved by spin coating[27] or when electrostatic interactions[28] are involved. On the other hand, chemical grafting, resulting in much more stably anchored layer, can easily lead to proteins denaturation. This is the reason why we have chosen approaches such as the spin-coating and the LbL assemblies, that allow to obtain rather stably anchored but still functional biodeposits as demonstrated in previously published works. Here the morphology of the differently deposited SA layers was investigated by combining SEM and XSR analyses, for characterizations at micro and nano scales, respectively.

SEM pictures of a spin-deposited SA film are reported in Figure 2A,B showing that, at the μm length scale, SA molecules aggregate into clusters of different size (>1 μm), exhibiting an island-like structure, with features that are inhomogeneous in size and distributions. A single protein agglomerate is seen, at higher magnification, in Figure 2C, showing the expected irregular structure having regions with uneven height ranging from 1 to 2 μm.[25] The SA proteins assemble into clusters under spin-coating most probably because the deposition is carried out at very low rotational velocity resembling more a cast-deposition, known to produce such agglomerates.[29] The large degree of surface irregularity of the spin-deposited SA layer can be inferred also from the XSR curves that feature no interference (Kiessig) fringes (Figure S1). However, the presence of a thin streptavidin layer, in direct contact with the SiO_2 surface, acting as "ad-layer" or as a continuous system of "seeds" that promotes the growth of the larger agglomerates cannot be excluded. Such a structure could act as a continuous ionic conduction path between larger SA clusters and this explains why a consistently higher off-current is measured in FBI-OFETs in the presence of the protein layer.

Although the LbL deposited layer looks, at visual and optical microscope inspection, overall smoother than the spin-coated

dx.doi.org/10.1021/jp504652u | J. Phys. Chem. C 2014, 118, 15853−15862

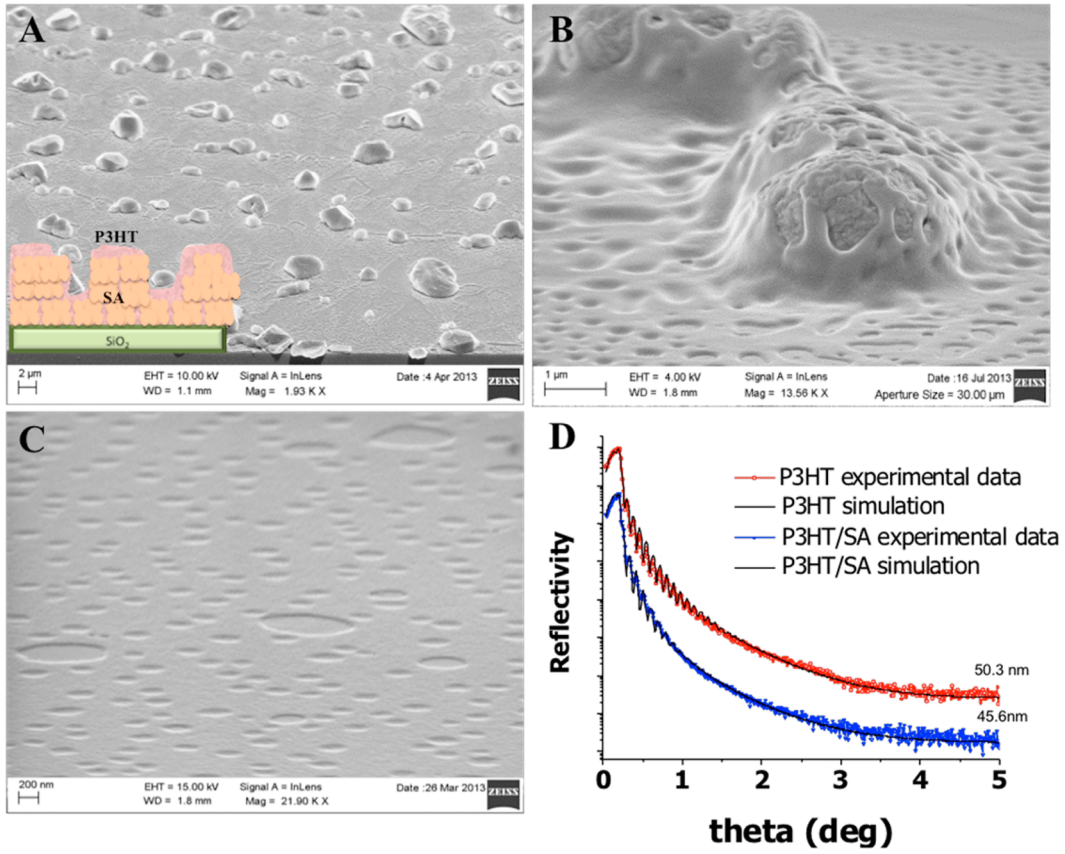

Figure 4. SEM images of a spin-coated SA layer covered by the P3HT organic semiconductor film. The sample was prepared by spin-coating a 10 μg/mL SA solution followed by P3HT at 2.5 μg/mL in chloroform. The images were acquired by tilting the sample of 60° (A) and 75° (B) at different magnifications; (C) SEM image of a P3HT film deposited by spin-coating on a bare Si/SiO_2 substrate, the image was acquired by tilting the sample of 75°; (D) XSR experimental (symbols) and simulated (lines) curves from a bare P3HT film (red curve) and a SA/P3HT bilayer obtained by spin-coating a 10 μg/mL SA solution and P3HT at 2.5 μg/mL in chloroform (blue curve). The actual thickness values as derived from the fit are reported next to each curve.

one, SEM measurements show that agglomerates of different sizes characterize also this kind of deposits. In Figure 3A, the PDDA adhesion polymer layer is imaged, showing a very uniform morphology with very small features whose nature is associated with the very thin palladium metallization as it will be addressed later. The SEM images collected on the LbL SA film (Figure 3B) show the presence of larger hundreds of nm wide clusters as well as of much smaller aggregates that are not evident on the bare PDDA adhesion polymer layer. They could be due to the adsorption of protein clusters already present in solution. Indeed, dynamic light scattering (DLS) measurements reveal the presence in solution of large protein clusters. However, the *number* of these aggregates is extremely small compared with the free proteins (with a 6 nm diameter) and they are easily revealed by DLS only because the intensity of scattered light scales as the sixth power of the size. Such inhomogeneous structure is confirmed also by the XSR data analysis reported in Figure 3C. The XSR curves were collected on the single PDDA polymer deposited on SiO_2 (orange triangles) and on a PDDA/SA/PDDA/SA film (magenta squares). The lines are the best fitting curves. This is the stacked multilayer structure used as active layer in the OFET biosensor exhibiting remarkable detection limits down to 3 part per trillion.[12] The single thickness fringe characterizing both XSR spectra, which corresponds to an overall film thickness of about 1 nm, does not vary significantly even when a SA/PDDA/SA multilayer is added to the first PDDA layer. These results indicate that each deposition step does not generate a structure of compact and segregated stacked layers that would increase the film thickness progressively. Rather, it increases the density of the previous not dense and uniform deposit, eventually increasing the size of PDDA and SA islands (see also the discussion of GISAXS results in the following). This is plausible as it has been demonstrated that in the LbL assembly, interactions can occur either between the proteins and the polymer or among the proteins themselves, leading to the formation of aggregates (rather than single layers) especially if nonspecific electrostatic interactions are involved.[28,30,31] An illustration of the model for the morphological features in a SA LbL deposition is reported in Figure 3D.

Morphology and Structure of the Spin-Deposited SA/P3HT Layers. In Figure 4A,B the micromorphology of a spin-deposited SA, covered by a P3HT film, is shown. Agglomerates, up to few μm in size, very similar to those present in the spin-deposited SA films, are seen in Figure 4A. These structures, better visible at higher magnification (Figure 4B), reveal features easily ascribable to a SA agglomerate smoothly covered by a much thinner P3HT layer. Interestingly, a P3HT layer full of hollows and voids covers the SA cluster and indeed, inspecting within a hole, the structural features characteristic of a protein cluster can be seen. In Figure 4C the SEM image of a bare P3HT film reveals that the hollows are present also when the film is deposited directly on the SiO_2 surface. The pores in the P3HT film can be originated by the occurrence of

dx.doi.org/10.1021/jp504652u | J. Phys. Chem. C 2014, 118, 15853−15862

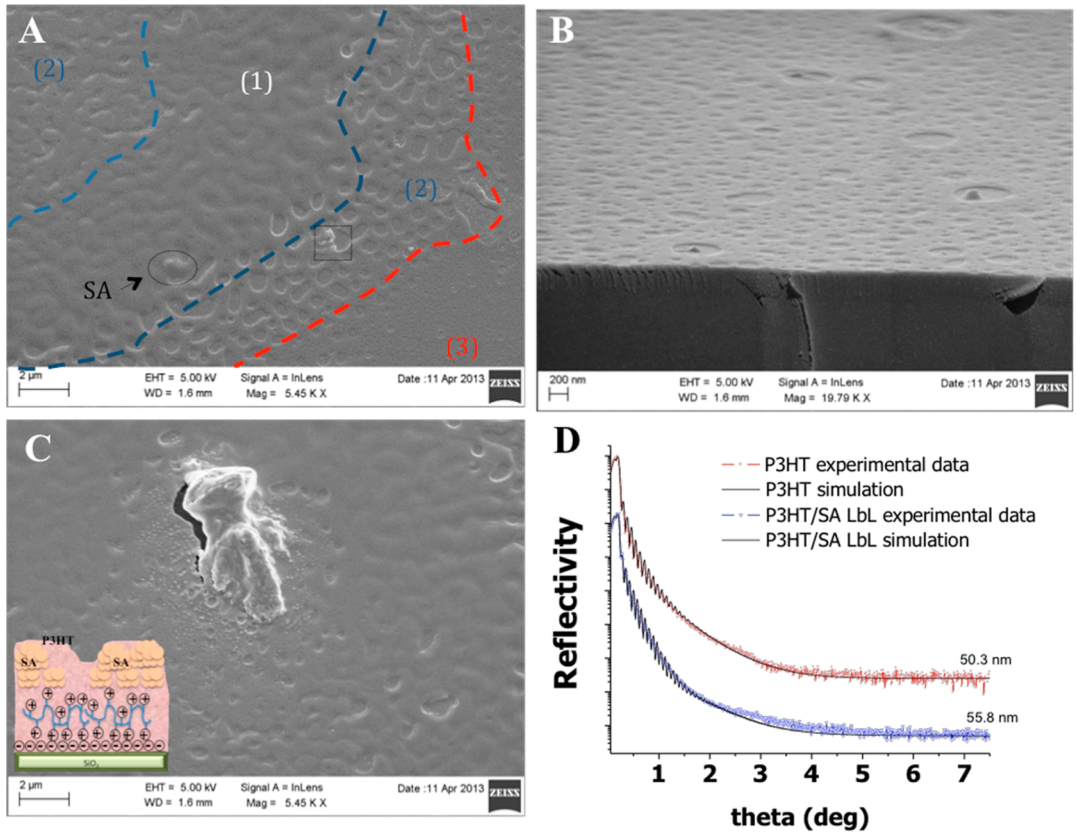

Figure 5. SEM images obtained for a sample formed by two layers of SA deposited by layer-by-layer assembly procedure on a Si/SiO_2 substrate and covered by the spin-deposited P3HT organic semiconductor film, the pictures were acquired by tilting the sample of 30° (A, B) and of 75° (C); (d) XSR experimental (symbols) and simulated (lines) curves from a bare P3HT film (red curve) and a SA/P3HT bilayer obtained by depositing SA by a layer by layer assembly procedure (blue curve). The actual thickness values as derived from the fit are reported next to each curve.

dewetting processes[32,33] that do take place when a hydrophobic organic semiconductor such as P3HT is deposited on hydrophilic surfaces such a not-silanized SiO_2 and a protein layer. It is in fact known that the silanizing process[20] improves the organic semiconductor adhesion on the SiO_2 surface. The presence of holes in the P3HT film having dimensions of ca. 10−100 nm was also confirmed by atomic force microscopy (AFM) as reported before.[9,12] However, the peculiar morphological features occurring in the P3HT film deposited on the SA layer works in favors of the FBI-OFET biosensors operation as it allows also rather large molecules, such as insulin or streptavidin, to percolate through the organic semiconductor film.[9] This was also confirmed by several experiments, based on luminescent techniques such as fluorescence and chemiluminescence.[9,12] A SEM analyses carried out on a device after 15 days shows that these morphological features are stably present in time. The P3HT layer structure evidence also that, notwithstanding the presence of holes, a continuous semiconductor layer spanning all the surface exists. Such a two-dimensional percolation of the P3HT domains sustains electronic paths explaining why the OFET electronic performances are only weakly affected in the SA FBI-OFET device.[12] In the light of these data it is also worth to comment on the field-effect mobility of the SA FBI-OFET being very close to that of the P3HT one. Indeed, the SA film surface roughness is much larger (>1 μm) than the average P3HT grain size (∼0.1 μm),[34,35] this allowing the charge carriers mobility (or delocalization length) of the P3HT not to be substantially affected as the film lies on the SA clusters.

The morphology of the SA/P3HT bilayer was also investigated by means of XSR. The reflectivity curves, collected on bare P3HT (red circles) and on the SA/P3HT bilayer (blu triangles) are shown in Figure 4D along with the best fittings curves (solid lines). Both curves presented show very similar features. The structure of the P3HT layer appears not affected by the presence of SA layer, and both the SA and SA/P3HT structures can be fitted with a single layer whose thickness is invariably ∼50 nm. These results lead to the conclusion that a P3HT film with an average thickness of 50 nm fills the space between the large aggregates, as evidenced by SEM. In such a space, only SA clusters smaller than 50 nm, embedded in the P3HT layer, are possibly allowed. A schematic of the bilayer structure is reported in the inset of Figure 4A. In Figure 4D the difference between model and experiment, around 2.65° (corresponding to 1.6 nm *d*-spacing), in the upper curve, is due to the appearance of the (100) diffraction peak related to molecular order (crystallinity) in P3HT, not taken into account in the reflectivity calculations.

Morphology and Structure of the LbL-Assembled-SA/P3HT Structures. In Figure 5 the SEM pictures of the LbL assembled SA layer, covered by the spin-coated P3HT film, are shown. In Figure 5A areas with different morphologies can be identified. The area (1) is characterized by a structured morphology where features ascribable to SA clusters covered by a voids free P3HT can be identified. In region (2) large pores are present, along with protruding SA agglomerates. Region (3) is characterized by small hollows (100 nm) and very uniform morphology. As shown in Figure 5B most of the SA clusters are

dx.doi.org/10.1021/jp504652u | J. Phys. Chem. C 2014, 118, 15853−15862

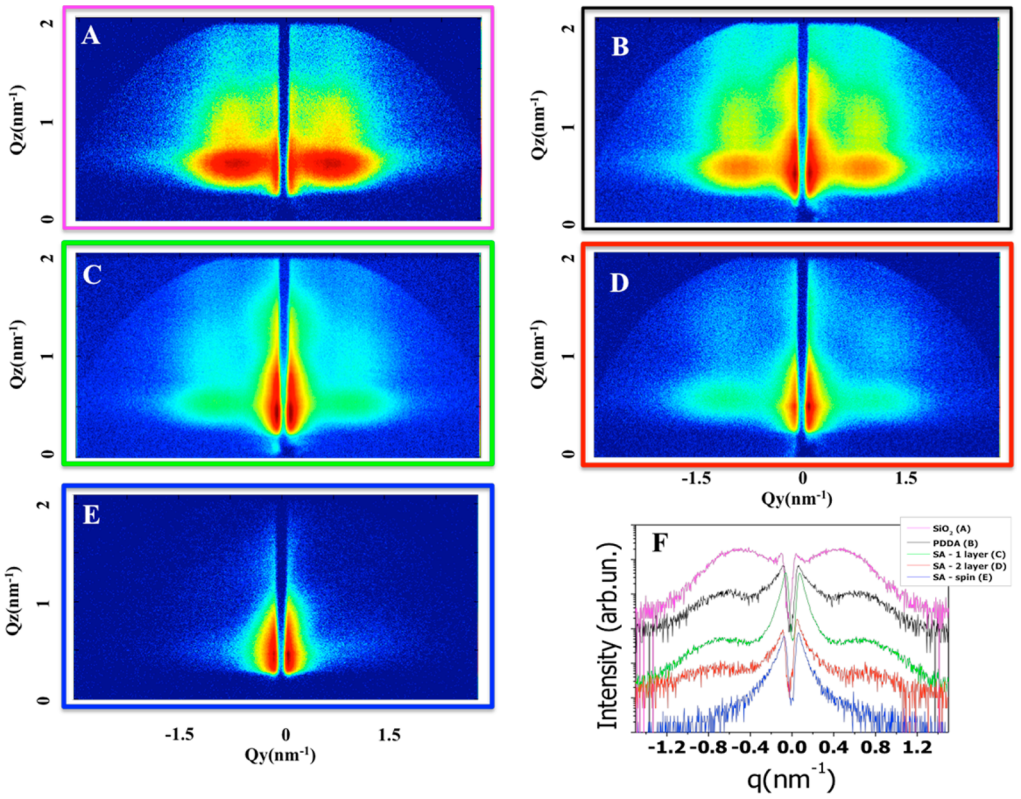

Figure 6. GISAXS patterns obtained for the bare Si/SiO_2 substrate (A); PDDA adhesion polymer deposited by LbL on a Si/SiO_2 substrate (B); one SA layer (C) and two SA layers (D) deposited by LbL on a Si/SiO_2 substrate; SA deposited by spin-coating on Si/SiO_2 substrate (E); (F) horizontal cuts taken in the 2D maps (a-e as specified in the legend) across the correlation peaks. Before the GISAXS analysis, a 10 nm palladium layer was evaporated on all the sample.

completely coated by the P3HT film, which also holds for large SA clusters protruding out of the P3HT surface (see Figure 5C). Moreover, since most of the SA clusters are of ca. 100 nm in size (Figure 3B), the SA layer cannot be planarized by a few tens of nm thick P3HT film, which on the other hand covers the entire surface of most of the clusters and fills the gap between them. The XSR curves in Figure 5D show, also for these samples, interference features that are invariably ascribable to a single layer with a thickness of ~50 nm, confirming the picture coming from the SEM analysis. Therefore, spin-deposited and LbL assembled SA layer (covered by P3HT) form structures composed of larger protein features that are connected by a 50 nm polymeric layer that grows in between and contains the smaller protein clusters.

GISAXS Analysis of the SA and SA/P3HT Layers. The GISAXS sensitivity was enhanced by coating the SA deposits with a thin palladium layer. In Figure 6A the GISAXS data from a Pd-coated SiO_2 substrate are reported, showing the typical scattering pattern from correlated particles uniformly distributed—on a smooth surface - with an average mutual distance (13.5 nm), comparable to their own diameter. These features are here ascribable to the nanostructured Pd film. Figure 6B-E show how the correlated structures vary with the investigated samples, being affected by surface modification, until vanishing completely in the case of spin-deposited SA. Precisely, for the LbL SA, the reference surface is the PDDA polymer deposit, whose GISAXS plot (Figure 6B) shows scattering features ascribable to evenly distributed Pd nanoparticles with a smaller correlation distance (10.3 nm) than that characterizing the Pd-coated SiO_2 surface (Figure 6A). The presence of these Pd nanoparticles is also confirmed by the SEM image reported in Figure 3A. In the case of the PDDA/SA (Figures 6C) and PDDA/SA/PDDA/SA (Figures 6D) LbL assemblies a further shift in the correlation peak positions toward larger q-values (smaller d-spacings) was found (9.2 and 8.4 nm, respectively). At the same time, a decrease in the correlation peak intensities was observed. The data measured on a metallized spin-coated SA layer (Figure 6E) show X-ray intensity concentrated in the very low scattering vectors region, this meaning that the signal coming from the correlated Pd nanoparticles is lost in this case.

In Figure 6F, the 1D profiles obtained from horizontal cuts taken in the 2D maps across the correlation peaks are reported to show the evolution of these features (peak intensity and position), as a function of the sample. Since such scattering features are typical of in plane-correlated objects formed on a smooth surface (SiO_2 or PDDA layers), and based on the conclusion drawn from SEM/XSR analyses (Figure 3) that no SA flat layers are formed in the PDDA/SA/PDDA/SA structure, it follows that the actual smooth surface cannot be provided by SA molecules but by the PDDA layer. Additionally, the q-shift and the intensity decrease of the correlation peaks can be then ascribed to the progressive covering of the surface by the protein material, with a certain fraction of free space being left between SA larger agglomerates, which in the case of LbL assemblies is not completely filled even after two deposition steps. On the other hand, the Pd nanoparticles correlation is significantly disrupted in the case of spin-deposited SA (Figure 6E), which indirectly proves that the spin-deposited SA layer largely covers the SiO_2 surface. It can

dx.doi.org/10.1021/jp504652u | J. Phys. Chem. C 2014, 118, 15853−15862

be therefore concluded that a good SA coverage of the Si/SiO_2 surface is achieved only after the two LbL depositions while it is already good after the spin SA deposition. This characterization rather clearly shows that the LbL deposit is much more regular and smooth than the spin-deposited one.

GIWAXS Investigation of P3HT Deposited on SA Layers. All the P3HT films deposited either directly on Si/SiO_2 substrates, or on SA-coated substrates show edge-on preferential orientation,[36] so that no significant structural differences are observed for films deposited directly on SiO_2 (or $PDDA/SiO_2$), on LbL-SA, or on spin-deposited SA. A typical GIWAXS pattern is shown in Figure 7 which indicates

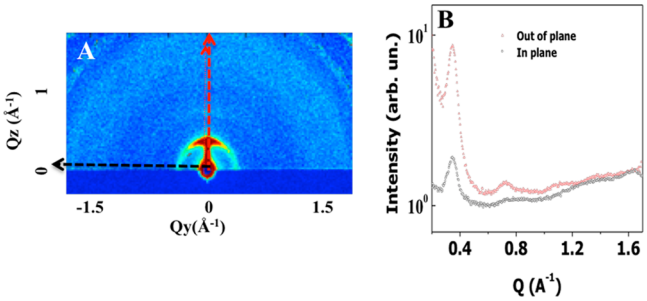

Figure 7. GIWAXS pattern obtained from a spin-deposited SA/P3HT bilayer, collected at 0.1° incidence angle: (A) 2D map; (B) linear cuts along the out of plane (q_z) and in plane (q_y) directions.

that the RR P3HT film grows with the ⟨100⟩ axis preferentially oriented normal to the film surface, according to a lamellar structure with a period of d=1.6 nm. This is in good agreement with published data for a high quality RR P3HT film.[37] The degree of preferential orientation was estimated by calculating the ratio between the (100) peak intensities in the vertical (approximately perpendicular to the substrate plane) and horizontal (in the substrate plane) directions indicated by the red and blue arrows in Figure 7A, respectively (after background subtraction). In Figure 7B the relevant linear cuts are reported. The computed ratio is always larger than 1, this clearly proving a high degree of edge-on to face-on orientations for P3HT on all kind of substrate. This is quite a relevant finding as it is well-known that the $\pi-\pi$ stacking for RR-P3HT resulting in the larger delocalization is with the polymer chains arranged edge-on on the substrate, clearly explaining why SA-FBI OFETs have the same mobility of a P3HT OFET.[9]

On the basis of the evidence gathered so far a possible model for the SA/P3HT system morphological and structural features comprises SA molecules aggregated into clusters of different size connected in a complex network mostly covered by the P3HT film. Such protein networks do not form uniform layers with large and flat interfaces, although the polyanionic polymer in the LbL deposition makes this deposit smoother, overall. The P3HT film that is subsequently deposited, leads to partial planarization of the SA features (in particular in LbL-SA), yielding anyhow to an inhomogeneous sieve-like surface. However, the P3HT retains the higher mobility edge-on structure also on the SA layer. The morphology of the P3HT covering layer allows also the percolation of large target molecules.

CONCLUSIONS

An extensive structural and morphological characterization of SA FBI-OFETs with a P3HT organic semiconductor is presented. The biological layer has been deposited by spin-coating and Layer-by-Layer deposition. The comparison between XSR curves and GISAXS patterns from SA layers indicate that a higher percentage of surface covering is obtained in the case of spin-deposited SA, being characterized by an irregular morphology and layer discontinuity. On the other hand a more homogeneous coating is obtained by a LbL deposition. This very well accounts for the better detection limits and overall analytical performances quality, measured on the LbL compared to the spin coated SA FBI-OFET sensors.[12] This assessment is also confirmed by the SEM analysis showing the degree of SA layer homogeneity at different length scales. Combined SEM, XSR, and GISAXS/GIWAXS studies of spin-coated SA samples covered by a P3HT film or by a thin metal layer allowed the investigation of SA and P3HT morphology, as well as of their stacked structure. The resulting overall picture of the FBI-OFET architecture consists in a discontinuous layer of SA agglomerates of different size locally forming, at different length scales, 3D islands, 2D patches or nanoscale networks, with thickness and branching increasing with SA surface coverage, until forming a compact layer in the case of spin-deposited SA. Here, an extended bilayer structure is formed, although with irregular morphology, after coating the SA film with the P3HT layer. On the other hand, the LbL-SA deposit features short-range paths with bilayer structures similar to the SA ramifications, which should be effective in the sensing mechanism of the FBI-OFET device. Importantly, the molecular structural arrangement of the P3HT film show a marked edge-on orientation on all the SA layer studied, giving a clear rationale for the consistently observed field-effect mobility invariance values measured on the SA FBI-OFETs. Last but not least, the clear evidence for large voids present in the P3HT layer, covering the SA deposit, explains why even large proteins such insulin or even streptavidin have been seen to actually percolate through the P3HT thin film. These last two features definitely confirm the wide applicability of the FBI-OFET sensing platform also to detect large target molecules.

ASSOCIATED CONTENT

Supporting Information

XSR analysis of a SA sample deposited by spin-coating on a SiO_2 substrate. This material is available free of charge via the Internet at http://pubs.acs.org.

AUTHOR INFORMATION

Corresponding Authors

*Phone: +390805929167. Fax: +390805929170. E-mail: cinzia.giannini@ic.cnr.it.

*Phone/Fax: +390805442092. E-mail: luisa.torsi@uniba.it.

Author Contributions

‖These authors contributed equally.

Notes

The authors declare no competing financial interest.

ACKNOWLEDGMENTS

Part of this work has been supported by the project Nanomax-integrable sensors for pathological biomarkers diagnosis (N–CHEM). The PON project "Laboratorio per lo Sviluppo Integrato delle Scienze e delle Tecnologie dei Materiali Avanzati e per dispositivi innovativi -LABORATORIO SISTEMA" by the Italian MIUR (Ministry of Education, Universities and Research) is acknowledged for partial support.

R. Lassandro is acknowledged for his full technical support with the XMI-LAB laboratory.

■ ABBREVIATIONS

OFET, organic field effect transistor; FBI, functional biological interlayer; SA, streptavidin; LbL, layer by layer deposition; OSC, organic semiconductor; P3HT, poly(3-hexylthiophene); SEM, scanning electron microscopy; XSR, X-ray specular reflectivity; GIWAXS, grazing incidence wide-angle X-ray scattering; GISAXS, grazing incidence small-angle X-ray scatter-ing; PDDA, poly(diallyldimethylammonium chloride)

■ REFERENCES

(1) Lin, P.; Yan, F. Organic Thin-Film Transistors for Chemical and Biological Sensing. *Adv. Mater.* **2012**, *24*, 34−51.
(2) Torsi, L.; Magliulo, M.; Manoli, K.; Palazzo, G. Organic Field-Effect Transistor Sensors: A Tutorial Review. *Chem. Soc. Rev.* **2013**, *42*, 8612−28.
(3) Svennersten, K.; Larsson, K. C.; Berggren, M.; Richter-Dahlfors, A. Organic Bioelectronics in Nanomedicine. *Biochim. Biophys. Acta* **2011**, *1810*, 276−285.
(4) Kang, B.; Lee, W. H.; Cho, K. Recent Advances in Organic Transistor Printing Processes. *ACS Appl. Mater. Interfaces* **2013**, *5*, 2302−2315.
(5) Di, C. A.; Zhang, F.; Zhu, D. Multi-functional Integration of Organic Field-Effect Transistors (OFETS): Advances and Perspectives. *Adv. Mater.* **2013**, *25*, 313−330.
(6) Khan, H. U.; Roberts, M. E.; Johnson, O.; Forch, R.; Knoll, W.; Bao, Z. In Situ, Label-Free DNA Detection Using Organic Transistor Sensors. *Adv. Mater.* **2010**, *22*, 4452−4456.
(7) Hammock, M. L.; Knopfmacher, O.; Naab, B. D.; Tok, J. B. H.; Bao, Z. Investigation of Protein Detection Parameters Using Nanofunctionalized Organic Field-Effect Transistors. *ACS Nano* **2013**, *7*, 3970−3980.
(8) Torsi, L.; Farinola, G. M.; Marinelli, F.; Tanese, M. C.; Omar, O. H.; Valli, L.; Babudri, F.; Palmisano, F.; Zambonin, P. G.; Naso, F. A Sensitivity-Enhanced Field-Effect Chiral Sensor. *Nat. Mater.* **2008**, *7*, 412−417.
(9) Angione, M. D.; Cotrone, S.; Magliulo, M.; Mallardi, A.; Altamura, D.; Giannini, C.; Cioffi, N.; Sabbatini, L.; Fratini, E.; Baglioni, P.; et al. Interfacial Electronic Effects in Functional Biolayers Integrated into Organic Field-Effect Transistors. *Proc. Natl. Acad. Sci. U.S.A.* **2012**, *109*, 6429−6434.
(10) González, M.; Bagatolli, L. A.; Echabe, I.; Arrondo, J. L. R.; Argaraña, C. E.; Cantor, C. R.; Fidelio, G. D. Interaction of Biotin with Streptavidin. Thermostability and Conformational Changes upon Binding. *J. Biol. Chem.* **1997**, *272*, 11288−11294.
(11) Macchia, E.; Giordano, F.; Magliulo, M.; Palazzo, G.; Torsi, L. An Analytical Model for Bio-Electronic Organic Field-Effect Transistor Sensors. *Appl. Phys. Lett.* **2013**, *103*, 103301.
(12) Magliulo, M.; Mallardi, A.; Gristina, R.; Ridi, R.; Sabbatini, L.; Cioffi, N.; Palazzo, G.; Torsi, L. Part-Per-Trillion Label-Free Electronic Bio-Analytical Detection. *Anal. Chem.* **2013**, *85*, 3849−3857.
(13) Ariga, K.; Hill, J. P.; Ji, Q. Layer-By-Layer Assembly as a Versatile Bottom-Up Nanofabrication Technique for Exploratory Research and Realistic Application. *Phys. Chem. Chem. Phys.* **2007**, *9*, 2319−2340.
(14) Steen Redeker, E.; Ta, D. T.; Cortens, D.; Billen, B.; Guedens, W.; Adriaensens, P. Protein Engineering for Directed Immobilization. *Bioconjugate Chem.* **2013**, *24*, 1761−1777.
(15) Sirringhaus, H. 25th Anniversary Article: Organic Field-Effect Transistors: The Path Beyond Amorphous Silicon. *Adv. Mater.* **2014**, *26*, 1319−1335.
(16) Newbloom, G. M.; Kim, F. S.; Jenekhe, S. A.; Pozzo, D. C. Mesoscale Morphology and Charge Transport in Colloidal Networks of Poly(3-hexylthiophene). *Macromolecules* **2011**, *44*, 3801−3809.
(17) Di, C.-a.; Liu, Y.; Yu, G.; Zhu, D. Interface Engineering: An Effective Approach Toward High-Performance Organic Field-Effect Transistors. *Acc. Chem. Res.* **2009**, *42*, 1573−1583.
(18) Urien, M.; Wantz, G.; Cloutet, E.; Hirsch, L.; Tardy, P.; Vignau, L.; Cramail, H.; Parneix, J.-P. Field-Effect Transistors Based on Poly(3-Hexylthiophene): Effect of Impurities. *Org. Electron.* **2007**, *8*, 727−734.
(19) Välimaa, L.; Pettersson, K.; Rosenberg, J.; Karp, M.; Lövgren, T. Quantification of Streptavidin Adsorption in Microtitration Wells. *Anal. Biochem.* **2004**, *331*, 376−384.
(20) Salleo, A.; Chabinyc, M. L.; Yang, M. S.; Street, R. A. Polymer Thin-Film Transistors with Chemically Modified Dielectric Interfaces. *Appl. Phys. Lett.* **2002**, *81*, 4383−4385.
(21) Pietsch, U.; Holy, V.; Baumbach, T. In *High Resolution X-Ray Scattering: from Thin Films to Lateral Nanostructures*, 2nd ed.; Springer: Berlin, 2004.
(22) Cassiers, T.; Lowack, K.; Decher, G. Layer-By-Layer Assembled Protein/Polymer Hybrid Films: Nanoconstruction via Specific Recognition. *Supramol. Sci.* **1998**, *5*, 309−315.
(23) Altamura, D.; Lassandro, R.; Vittoria, F. A.; De Caro, L.; Siliqi, D.; Ladisa, M.; Giannini, C. X-Ray Microimaging Laboratory (XMI-LAB). *J. Appl. Crystallogr.* **2012**, *45*, 869−873.
(24) González, M.; Bagatolli, L. A.; Echabe, I.; Arrondo, J. L. R.; Argaraña, C. E.; Cantor, C. R.; Fidelio, G. D. Interaction of Biotin with Streptavidin: Thermostability and Conformational Changes upon Binding. *J. Biol. Chem.* **1997**, *272*, 11288−11294.
(25) Bhushan, B.; Tokachichu, D. R.; Keener, M. T.; Lee, S. C. Morphology and Adhesion of Biomolecules on Silicon Based Surfaces. *Acta biomater.* **2005**, *1*, 327−341.
(26) Eteshola, E.; Keener, M. T.; Elias, M.; Shapiro, J.; Brillson, L. J.; Bhushan, B.; Lee, S. C. Engineering Functional Protein Interfaces for Immunologically Modified Field Effect Transistor (Immunofet) by Molecular Genetic Means. *J. R. Soc. Interface* **2008**, *5*, 123−127.
(27) Muller-Buschbaum, P.; Gebhardt, R.; Maurer, E.; Bauer, E.; Gehrke, R.; Doster, W. Thin Casein Films as Prepared by Spin-Coating: Influence of Film Thickness and of pH. *Biomacromolecules* **2006**, *7*, 1773−1780.
(28) Ladam, G.; Schaaf, P.; Cuisinier, F. J. G.; Decher, G.; Voegel, J.-C. Protein Adsorption onto Auto-Assembled Polyelectrolyte Films. *Langmuir* **2001**, *17*, 878−882.
(29) Gebhardt, R.; Vendrely, C.; Burghammer, M.; Riekel, C. Characterization of the Boundary Zone of a Cast Protein Drop: Fibroin β-Sheet and Nanofibril Formation. *Langmuir* **2009**, *25*, 6307−6311.
(30) Ladam, G.; Gergely, C.; Senger, B.; Decher, G.; Voegel, J.-C.; Schaaf, P.; Cuisinier, F. J. G. Protein Interactions with Polyelectrolyte Multilayers: Interactions between Human Serum Albumin and Polystyrene Sulfonate/Polyallylamine Multilayers. *Biomacromolecules* **2000**, *1*, 674−687.
(31) Salloum, D. S.; Schlenoff, J. B. Protein Adsorption Modalities on Polyelectrolyte Multilayers. *Biomacromolecules* **2004**, *5*, 1089−1096.
(32) Xu, L.; Sharma, A.; Joo, S. W. Instability and Pattern Formation Induced in Thin Crystalline Layers of a Conducting Polymer P3HT by Unstable Carrier Films of an Insulating Polymer. *J. Phys. Chem. C* **2012**, *116*, 21615−21621.
(33) Bandyopadhyay, D.; Sharma, A.; Rastogi, C. Dewetting of the Thin Liquid Bilayers on Topographically Patterned Substrates: Formation of Microchannel and Microdot Arrays. *Langmuir* **2008**, *24*, 14048−14058.
(34) Lovinger, A. J.; Davis, D. D.; Ruel, R.; Torsi, L.; Dodabalápur, A.; Katz, H. E. Morphology of α-Hexathienyl Thin-Film-Transistor Films. *J. Mater. Res.* **1995**, *10*, 2958−2962.
(35) Torsi, L.; Dodabalapur, A.; Lovinger, A. J.; Katz, H. E.; Ruel, R.; Davis, D. D.; Baldwin, K. W. Rapid Thermal Processing of α-hexathienylene Thin-Film-Transistors. *Chem. Mater.* **1995**, *7*, 2247−2251.
(36) Aryal, M.; Trivedi, K.; Hu, W. Nano-Confinement Induced Chain Alignment in Ordered P3HT Nanostructures Defined by Nanoimprint Lithography. *ACS Nano* **2009**, *3*, 3085−3090.

(37) Noriega, R.; Rivnay, J.; Vandewal, K.; Koch, F. P. V.; Stingelin, N.; Smith, P.; Toney, M. F.; Salleo, A. A General Relationship Between Disorder, Aggregation and Charge Transport in Conjugated Polymers. *Nat. Mater.* **2013**, *12*, 1038−1044.